Journal of Materials Chemistry C

Accepted Manuscript

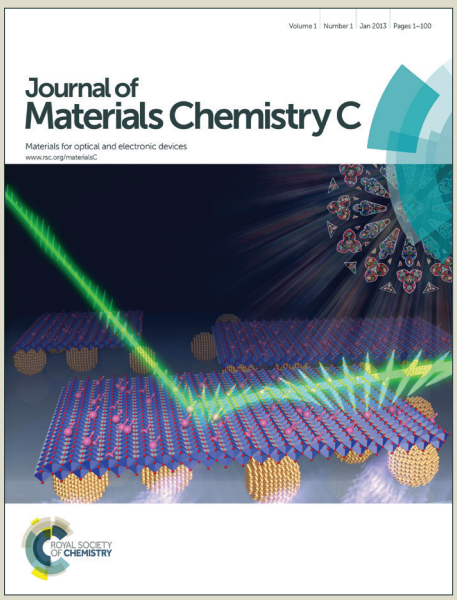

ROYAL SOCIETY OF CHEMISTRY

www.rsc.org/materialsC

Journal Name Journal of Materials Chemistry C Dynamic Article Links ►

Cite this: DOI: 10.1039/c0xx00000x

www.rsc.org/xxxxxx

ARTICLE TYPE

Highly Crystalline and Ordered Nanoporous SnO_2 Thin Films with Enhanced Acetone Sensing Property at Room Temperature

Shaofeng Shao,*[a] Hongyan Wu,[a] Shimin Wang,[a] Qiling Hong,[a] Ralf Koehn,[b] Tao Wu[a] and Wei-Feng Rao[a]

Received (in XXX, XXX) Xth XXXXXXXXX 20XX, Accepted Xth XXXXXXXXX 20XX

DOI: 10.1039/b000000x

Gas sensing with highly ordered nanoporous materials is attracting much attention because of its promising capability of detecting toxic gases at room temperature. In this study, highly organized, transparent, crystalline nanoporous Pd-doped SnO_2 thin films are obtained through a 120 °C post-synthetic water vapour hydrothermal treatment of the as-deposited film. Characterizations by XRD, SEM, TEM, HRTEM, Raman spectroscopy and XPS reveal that Pd-doped SnO_2 thin film obtained highly ordered nanostructure, highly crystalline tin oxide of cassiterite structure, small particle size, and outstanding particle interconnectivity. The best results with respect to porosity, nanostructured ordering, as well as the sensing behaviour are obtained by the tin dioxide thin films doped with 4 wt% palladium prepared with spin-coating at 30% relative humidity, aging for 2 h at 60°C, for 12 h at 120°C and 95% relative humidity and gradual calcination at 300°C. The acetone response of the SnO_2 sensing film with 4 wt% Pd-doping level is found to be substantially improved up to 14.64 at 100 ppm with a short response time of ~30 s at room temperature. In general the synthesis procedure described in this report has the advantage of being easy, cost efficient, highly reproducible and therefore highly suitable for the fabrication of high performance ordered nanoporous crystalline materials for applications including gas sensing, photocatalysis, and 3rd generation photovoltaics.

1. Introduction

Environmental pollution is a critical problem that affects our health as it causes cancers, birth defects, and mental retardation. Among the contaminants in air, volatile organic compounds (VOCs), such as benzene, acetone, and toluene, are the most common and dangerous because they not only pollute the environment but also directly affect human's health. For instance, acetone is believed to exhibit only a slight toxicity with normal use, but its hazard lies in its extreme flammability. The materials safety data sheet of acetone announces that at a temperature higher than flash point (-20°C), air mixtures of between 2.5% and 12.8% acetone by volume may explode or cause a flash fire. Despite its toxicity and hazard, acetone is still used in industries as intermediates to produce other chemicals and as solvents in research laboratories. The probability of over exposure to such toxic agent is very high; therefore, the development of gas sensors for early detection of flammable and/or toxic gases in necessary. [1-4]

Over the past several decades, metal oxide nanomaterials, such as ZnO[2], WO_3[5], SnO_2[3], and In_2O_3[6, 7], have been fabricated for detecting acetone due to their stable chemical transduction properties, which can reversibly convert chemical interaction on a surface to change the electrical conductivity. Among the metal oxides, tin dioxides are especially promising, due to their attractive chemicophysical properties, including a lower toxicity and high availability. SnO_2 based gas sensors have been prepared by a variety of methods, such as sol-gel, chemical vapour deposition, magnetron sputtering, sonochemical, and thermal evaporation. Although many investigations have reported great potential for SnO_2 based sensors for detecting VOCs[8], some specific problems hindered their applications, such as high operation temperatures, short sensor life and high power consumption, and produce challenging obstacles for achieving low power consumption towards practical applications.

Porous metal oxide films with high surface areas have attracted a great deal of attention due to their wide range of application as adsorbents for environmentally hazardous chemicals, reaction catalysts, chemical sensors, and electrical and optical devices. To achieve rapid oxidation/reduction elevated temperature above 200 °C or UV light is needed for a practical and sensitive acetone detector.[9-13] Recently, there have been relatively few reports on the SnO_2 based thin films exhibiting high sensitivity towards acetone at room temperature.[14, 15] However, these thin films did not exhibit highly ordered mesotructure nor was any mesoporosity investigated and the sensor response was slower than for the palladium-doped sensors.[11] Extensive studies have revealed critical factors that govern the gas-sensing properties of nanoporous SnO_2 thin films. Specifically, the following three factors have been proposed as being the most influential: ordered nanostructure, crystalline size, and surface modification (noble metal loading).

Ordered nanoporous metal oxides can be directly synthesized

by the cooperative assembly of inorganic metal precursors and organic surfactants, also called soft-template method via a sol-gel process.[16-18] Meanwhile, non-template synthetic methods have also been reported to prepare nanoporous metal oxides.[19-21] Toupance et al. have set up a new organometallic solution route toward self-assembled organotin-based hybrid thin films based on the design of suitable sol−gel precursors.[22] Thus, nanoporous organotinbased hybrid thin films showed unexpected selectivity for hydrogen gas sensing at moderate temperature.[23, 24] Futhermore, UV-treated or calcined hybrid thin films yielded excellent sensitivity toward hydrogen and carbon monoxide.[25] However, the above methods have been limited because of the poor nanoscale phase separation during the framework crystallization, which leads to loss of nanostructured definition. Post-synthetic hydrothermal treatment is an efficient approach for synthesis of highly ordered crystalline nanoporous metal oxide, because the synthetic approach overcomes the problems for the so far established methods. It allows the synthesis of metal oxide thin films with ordered nanopores at low temperature. Furthermore, crystalline pore walls can be achieved at low temperatures allowing an easy thermal removal of the template by calcination without loss of nanoporous structure or significant shrinkage of the thin film normal to the substrate. It is knowledge that the nanostructure of the ordered nanoporous metal oxides plays an important role in their application performance. The post-synthetic water vapour hydrothermal treatment provides an effective way to research the effect mechanism of nanostructured ordering and particle size of nanoporous metal oxides on their corresponding application property.

On the other hand, according to the sensing mechanisms of gas sensors, the performance is greatly influenced by crystalline size of SnO_2 material.[8] Xu et al. reported that the sensor response drastically increased as the crystal size decreased to less than 6 nm, which is twice as large as the thickness of depletion layers in SnO_2.[26] When the thickness of depletion layers becomes comparable to the crystal radius, electron depletion layers form over the crystals, significantly increasing the difference in the electric resistance between in air and in target gases. The crystal size effect on the sensor response has recently been remodelled by Yamazoe et al.,[27, 28] who postulated a new type of electron depletion designated "volume depletion", which occurs upon decreasing the crystallite size and donor density as well as increasing the oxygen partial pressure. When reducing gases react with the adsorbed oxygen, a highly electron depleted state disappears, generating a large change in the electrical resistance, i.e., large sensor response. Thus, decreasing the crystallite size of SnO_2 is another one of the efficient ways to obtain high sensitivity (sensor response).

Another way to improve the sensor response is surface modification. Generally, loading metals or metal oxides such as Pd/PdO, and Pt on the SnO_2 surface increases the sensor response to combustible gases[29] and the gas selectivity[30]. Koziej et al. theoretically considered that Pd on the SnO_2 surface provides reaction sites for oxygen adsorption and combustion.[31] This is because the surface Pd can lower the energy barriers of the gas adsorption and gas dissociation, which catalytically facilitates combustion reactions. Electrical sensitization effects of Pd/PdO have also been revealed.[32] Additionally, doping with noble metals such as palladium is known to inhibit particle growth. [33] However, there has been little exploration of the Pd-doped ordered nanoporous SnO_2 in gas-sensing reactions.

Based on the above mentioned ways we developed a post synthetic hydrothermal treatment for the synthesis of highly ordered nanoporous Pd-SnO_2 sensing films, with homogeneous and controlled film thickness and the controllable pore size in our group. Briefly, an ethanolic solution containing a tin oxide precursor and dopant as well as an organic template is spin-coated onto a sensor device. Upon the treatment, the system co-assembles to form an inorganic/organic composite with nanoscale periodicity and crystalline nanoparticles. This composite is then thermally treated to remove the organic template and to further increase crystallinity of pore walls. The structure, crystallinity and composition of the ordered nanoporous Pd-SnO_2 thin films are characterized by HRTEM, FESEM, SAED, and STEM. It is found that the obtained thin films have highly crystallized nanoporous texture, small grain size (~3.2nm), and outstanding particle interconnectivity, making them promising candidates in preparing highly sensitive gas sensors. Importantly, the response time and the sensitivity of such ordered nanoporous films-based sensors were improved in a simply synthetic procedure by changing dopant concentrations and controlling grain size of the ordered nanoporous films. The best gas sensing result, a change of ~ 15 times of electrical resistance in response to 100 ppm acetone at room temperature, was obtained in the SnO_2 thin film doped with 4wt% Pd. It is well known that, besides the parameters of response time and the sensitivity, selectivity is another important issue for the sensing elements.[34] The gas-sensing properties of synthesized nanoporous films are investigated to volatile organic compounds (VOCs) such as toluene, acetone, isopropanol, ethanol, and aether at room temperature. The ordered nanoporous SnO_2 thin films have been found to be more effective in the detection of acetone.

2. Fabrication and measurement of sensors

2.1 Sensing Film Fabrication and Characterizations.

The Sn precursor solutions were prepared by dissolving 1 g $SnCl_4$ (Aldrich) in 0.153 mol ethanol in the presence of 3.83E-5 mol PluronicF127 triblock copolymer ([$(HO(CH_2CH_2O)_{106}$-$(CH_2CH(CH_3)O)_{70}$-$(CH_2CH_2O)_{106}H$, $EO_{106}PO_{70}EO_{106}$], Sigma). For Pd doping, 0.01g, 0.02g, 0.04g, and 0.08 g $PdCl_2$ (Aldrich) was dissolved in 1.80 ml 12 M HCl and then mixed with the above tin precursor solution under constant stirring for two days. The resulting (clear) Pd-Sn precursor solutions were stable over a one month period. The molar ratio of $SnCl_4$:F127:EtOH:$PdCl_2$:H-Cl:H_2O in the final Pd-Sn precursor solution was 1:0.01:40:(0.0147-0.1175):6:21. Gas sensing thin films were prepared by spin-coating 50 µl of the Pd-Sn precursor solution onto one sensor device of *ca*. 10 × 10 mm^2 with interdigital electrode at 4000 rpm for 90 s under 30% relative humidity for two times, and then dried at 60°C for 2 h. The films were then exposed to a water vapor hydrothermal treatment, 95% relative humidity, at 120°C for 12 h. The relative humidity was achieved using a supersaturated salt aqueous solution, kept at 120°C, in a humidity controlled chamber. The organic surfactant templates were then removed by annealing at temperatures of 300°C for 2 h with an up/down ramp rate of 1.0°C/min.

SAXRD patterns of the thin films were taken on an XDS-2000 diffractometer (Scintag Inc.) using Cu K radiation. WAXRD data were obtained by a Bruker D8 Advance X-ray diffractometer with Cu Ka (0.15406 nm) radiation. Field-emission scanning electron microscopy (FE-SEM, Hitachi S-4800) was used to observe the morphologies of the sensing films. Nitrogen sorption measurements were carried out at 77 K using a NOVA 4000e (Quantachrome Instruments) on Pd doped tin oxides scratched from several films. High resolution transmission electron microscopy (HRTEM) and scanning transmission electron microscopy in high angle annular dark field mode (STEM-HAADF) were performed using a FEI Titan 80-300 equipped with a field emission gun operated at 300 kV; film parts were scratched from the substrate and collected on an amorphous holey carbon film on a copper grid. XPS spectra were recorded using a Kratos Axis Ultra DLD spectrometer employing a monochromated Al-Ka X-ray source (hv= 1486.6 eV), hybrid (magnetic/electrostatic) optics and a multi-channel plate and delay line detector (DLD). Surface charging was corrected by referencing the spectra to C-C state of the C 1s peak at binding energy at 284.6 eV. All XPS spectra were recorded using an aperture slot of 300*700 microns, survey spectra were recorded with a pass energy of 160 eV, and high resolution spectra with a pass energy of 40 eV. XANES measurement was carried out at room temperature, at HASYLAB (HAmburg SYnchrotron radiation LABoratory) (4.5 GeV, 140 mA) Germany. Raman spectra were recorded with a LabRAM HR UV-vis (Horiba Jobin Yvon) Raman microscope (Olympus BX41) with a Symphony CCD detection system using a HeNe laser at 632.8 nm. The spectra were taken from material removed from the substrate.

2.2 Gas-Sensing Measurement

During the sensing measurement, liquid VOCs were inputted through a sample inlet and led down to a heater, which vaporized it. A fan ensured that the vapour was homogeneously distributed. The gas sensing properties were determined in a sample cell consists of a sample chamber and has a gas inlet and outlet, as shown in ESI, Fig S1. Resistance changes upon sample exposure to gases were recorded by a high resistance meter Keithley 6517A. The sensor response is defined as $S= (R_a-R_g)/R_g$, where R_a and R_g are the sensor resistances in air and in the target gas, respectively. Here, the response or recovery time is defined as the time taken for the sensor to achieve 90% of its maximum response or decreases to 10% of its maximum response, respectively.

3. Results and discussion

3.1 Material Properties

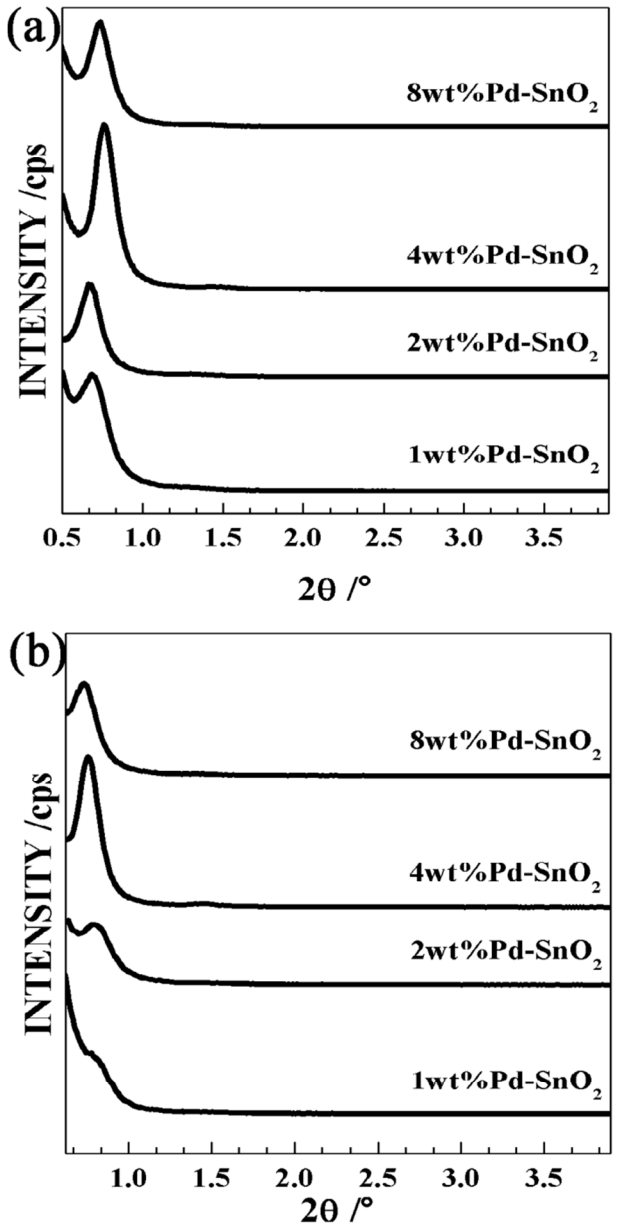

Fig. 1 Small-angle XRD patterns of nanoporous 1wt%, 2wt%, 4wt%, and 8wt% Pd-SnO_2 thin films synthesized after 120°C hydrothermal treatment (a) ; and annealing at 300°C (b).

Doping levels during the synthetic procedure have been proved to have great effect in the nanostructure ordering and particle size during the synthesis of nanoporous metal oxides. In this work, the research aim was to find the particular relation between the nanostructured ordering and particle size of ordered nanoporous SnO_2 and their gas sensing performance. For this purpose, four different nanoporous SnO_2 samples were synthesized with

controlled nanostructure and particle size. The crystallinity and structure of the synthesized thin films were examined by X-ray diffraction. For the as-synthesized air-dried Pd-SnO_2 thin films, no diffraction peaks were observed within the small angle X-ray diffraction (SAXRD) patterns (not shown for brevity), indicating a disordered nanostructure. An ordered nanostructure formed after exposing the Pd-SnO_2 thin films to the hydrothermal treatment (120°C, 12 h) was indicated by the peak appearing at ≈ 0.76° on the SAXRD pattern, Fig. 1a. The SAXRD patterns of the thin films of SnO_2 doped with different concentration of Pd are depicted in Fig. 1a: 1wt%, 2wt%, 4wt%, and 8wt%, respectively. All five films treated by hydrothermal treatment exhibit ordered nanostructures. The ordered nanostructure of the thin film is then retained through the progressive thermal treatment. After calcination at 300°C, as the concentration of Pd increases from 1wt% to 4wt%, in Fig. 1b, the diffraction peaks become sharper and stronger, and then the diffraction peak intensity decreases with further increase in the Pd concentration. The decrease of peak intensity can be interpreted as a reduction in the X-ray diffraction contrast between the pore and the framework,[35] revealing that the nanostructured ordering of SnO_2 can be varied by the change of Pd concentrations.

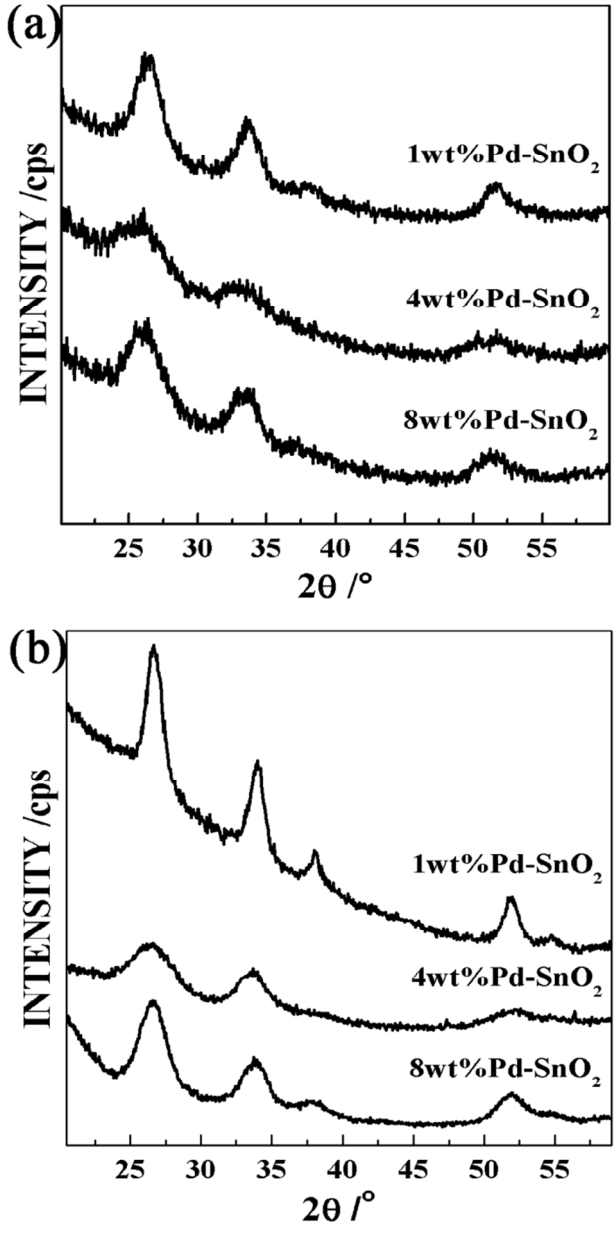

Fig. 2 XRD patterns of nanoporous 1wt%, 4wt%, and 8wt% Pd-SnO_2 thin films synthesized after 120°C hydrothermal treatment (a) ; and annealing at 300°C (b).

XRD patterns of post-synthetic water vapour hydrothermal treated 1-8 wt% Pd-doped SnO_2 sensing films are shown in Fig. 2a. The peak position and relative intensity of all diffraction peaks for the products match standard powder diffraction data (JCPDS 41-1445). The XRD pattern of the hydrothermal treated Pd-SnO_2 thin films exhibits five discrete *hkl* reflection at 26.6°, 33.9°, 38.0°, 51.8°, and 54.8°, respectively, corresponding to the (110), (101), (200), (211) and (220) crystallographic planes of tetragonal SnO_2 in accordance with the synthetic cassiterite. No

characteristic peaks belonging to other SnO_2 crystals or impurities were detected. All diffraction peaks in Fig. 2b became stronger and sharper with the 300°C heat treatments. The average crystalline grain size (D) calculated from the full width at half-maximum, FWHM, of the (110) reflection line using the Scherrer formula, [The average crystallite size (Ds) was obtained by $Ds=0.9*\lambda/(B*\cos\theta)$, where λ is the wavelength of X-ray ($\lambda_{Cu}=0.15418nm$) and B is the full-width at half-maximum of the XRD peak centered at 2θ degrees], is 3.2 nm for 4wt% Pd-SnO_2 thin film, 5.2 nm for 8wt% Pd-SnO_2 thin film and 8.3 nm for 1wt% Pd-SnO_2 thin film. However, peaks of Pd phase cannot be seen in these patterns due to possibly to the absence of crystalline PdO_x particles. The 300°C annealed 4wt% Pd-SnO_2 thin films exhibit an average grain size of near to 3nm, which Srivastava reports as being beneficial for enhanced acetone sensitivity.[11] In ESI, Fig. S2 shows the room-temperature Raman spectrum of the 4wt% Pd-SnO_2 thin films. The Raman shift peaks are 422, 463, 624, and 762 cm^{-1}, which are attributed to the A_{2g}, E_g, A_{1g}, and B_{2g} vibration modes of SnO_2, respectively,[36] whereas the Raman bands measured at 213, 230, and 355 cm^{-1} were not detected in the nanopowders or bulk SnO_2. Liu et al. have reported, besides the expected E_g and A_{1g} bands, Raman bands located at 213 and 230 cm^{-1} in SnO_2 nanomaterials, which were attributed to E_u (TO) and E_u (LO) active modes.[37] It is reasonable to assign the two volume modes to IR modes whose Raman activities are induced by the size effect, which are due to the smaller diameter of SnO_2 nanoparticles. The third broad peak at 355 cm^{-1} was also reported in extra-fine (3-5 nm) nanoparticle, while it was not observed in the bigger SnO_2 nanocrystal samples.[38] This attributed to relaxation of Raman selection rule by reduction the particle size, also by the high concentration of defects in surface site such as oxygen vacancies (OVs) and vacancy clusters.

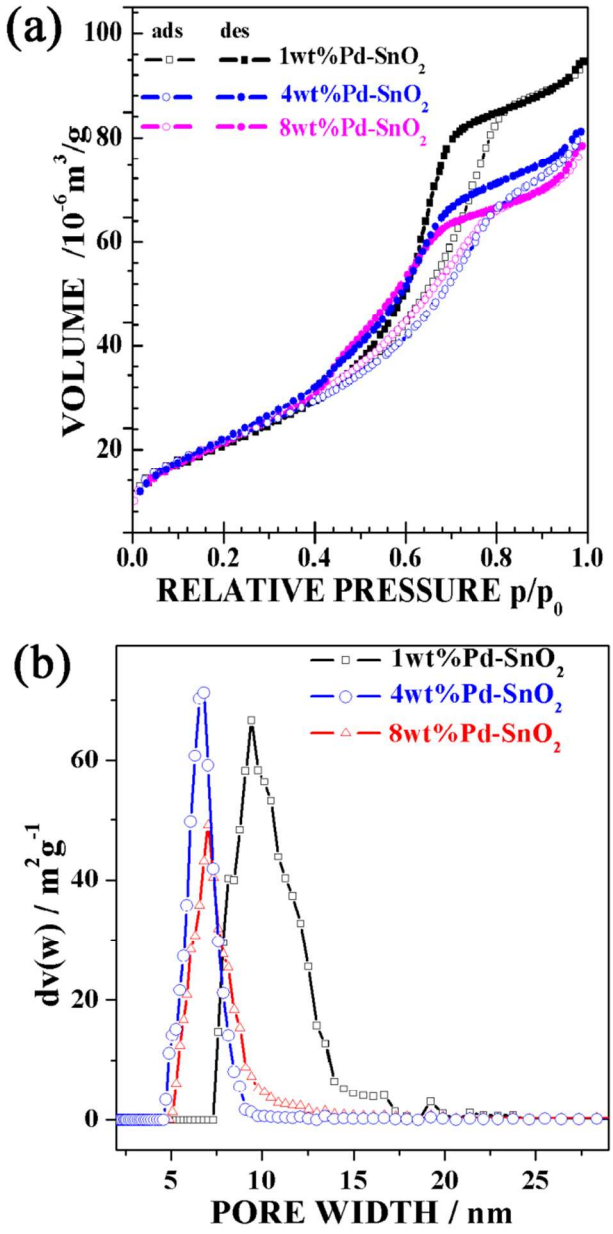

Fig. 3 (a) N_2 adsorption/desorption isotherms and (b) corresponding pore-size distribution for nanoporous 1wt%, 4wt%, and 8wt% Pd-SnO_2 thin films after 300°C anneal.

The porosity of tin dioxide thin films doped with 1wt%, 4wt%, and 8wt% Pd and heat-treated up to 300 °C were analysed from nitrogen adsorption-desorption isotherms. As shown in Fig. 3a, all SnO_2 samples gave typical IV isotherms, typical for the expected cylindrical nanopore shape. Clearly, with the increase of the concentration of dopant, the hysteresis loop occur at lower relative pressures, indicating smaller nanoporous diameters, a fact also substantiated by the pore size distributions calculated by Non-local Density Functional Theory (NLDFT) method (as shown in Fig. 3b).[39] The average pore size of 4wt% Pd-SnO_2

scratched thin films with one large hysteresis loop (P/P_0=0.4-1.0) is 6.5 nm, which arises from the piled porosity by aggregation of nanoparticles. For 1wt% Pd-SnO_2 and 8wt% Pd-SnO_2, the average pore sizes are 9.5 and 7.3, respectively, which can be compared to the average particle size obtained from the XRD patterns. It seems that the palladium doping is responsible for the narrower pore width distribution confirming the highly ordered uniform pore structure. As reported in the literature, palladium doping suppresses grain growth in bulk sol-gel systems.[40] The specific surface areas of 1wt%, 4wt%, and 8wt% Pd-SnO_2 scratched thin films are 88.6, 114.3, and 96.4 $m^2 g^{-1}$, respectively. As discussed above, for the ordered nanoporous thin films' synthesis, the concentration of Pd have a significant effect on the nanostructured ordering, particle size, surface areas, and pore size distribution of the nanoporous SnO_2. The 4wt% Pd-SnO_2 thin films show highest surface areas, smallest particle size, best nanostructured ordering, and narrowest nanopore distribution. In the following section, further discussion will be focus on the 4wt% Pd-SnO_2 thin films.

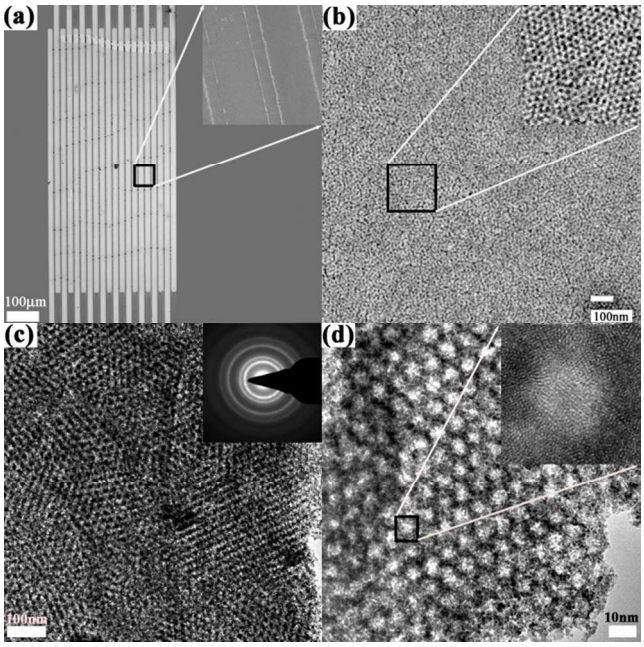

Fig. 4 (a) FESEM images of sensor device with the 300°C annealed ordered nanoporous 4wt% Pd-SnO_2 film; (b) FESEM images of the 300°C annealed nanoporous film; (c) TEM image of highly ordered nanoporous thin film annealed at 300°C. The inset shows SAED pattern of displayed area indicating the polycrystalline nature of the film; (d) TEM image of 300°C annealed ordered nanoporous 4wt% Pd-SnO_2 film. The inset is the HRTEM image of the rectangular marked region.

Fig. 4a shows the field emission (FE) SEM images of the sensor based on the ordered nanoporous 4wt% Pd-SnO_2 thin film. Interdigitated-finger arrays are clearly observed; the electrodes contain twenty fingers. Each finger is 10µm in width and 1mm in length, finger-finger spacing is 8µm, with a finger-to-finger overlap of 800µm. The enlarged image of the electrode shown in the inset of Fig. 4a indicates the deposition of the sensing film, which functions as a conducting channel and a sensing probe for the sensor measurements. As shown in Fig. 4b, the FESEM image of sensing thin films provides important information about the nanostructure of the thin films. It is seen that the nanoporous SnO_2 films possess excellent nanostructural regularity, which is important with respect to sensor devices, demanding crack-free coatings. Additionally, the images demonstrate that the nanopores are accessible from the top, enabling the diffusion of reactants into the porous framework.[41] The EDS spectrum collected from the Pd-doped SnO_2 sample shows the corresponding elemental mappings of Pd-doped SnO_2 in ESI, Fig.S3. It is seen that elements Sn, Pd, and O are distributed throughout sensing films, implying the SnO_2 formed a uniform chemical phase and the Pd component is homogeneously dispersed and is incorporated into the SnO_2 lattice. Fig. 4c shows a TEM image of a 300°C annealed nanoporous film, where the nanopore arrays are packed in an ordered arrangement with an average pore size of approximately 6-7 nm. Further information on the nanostructure of the thin film is provided by high resolution TEM (HRTEM) as shown in Fig. 4d. Nanostructural characteristic of the typical tetragonal SnO_2 thin films are further confirmed by the polycrystalline diffraction rings of the SAED pattern. It can be observed that the 300°C annealed nanoporous film is only composed of highly crystalline nanoparticles of cassiterite type, which is in good agreement with the wide-angle XRD studies (Fig. 2b). Obviously, the nanostructured ordering and particle size of the SnO_2 thin films can be controlled easily by the concentration of palladium. Cross-section TEM images shown in Fig. S4 reveal that all the SnO_2 samples have a network of nanopores. The particle sizes decreased and nanostructured ordering markedly increased with the increase of Pd concentrations from 1wt% to 4wt%, which is in good agreement with the SAXRD and WAXRD results. For 4wt% Pd-SnO_2 sample, one can see the presence of many interconnected nanoparticles with diameter near to 3nm and with long-range nanoporous periodicity, which means that the size of the nanostructured ordering is equal with the particle diameter.

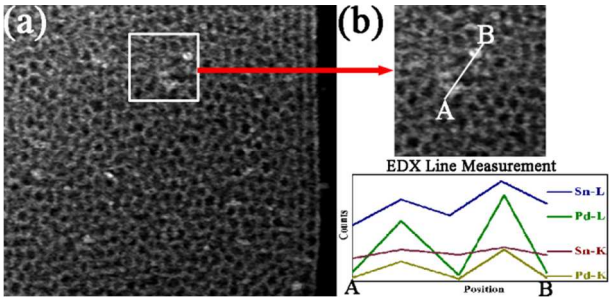

Fig. 5. a) Cross-section scanning transmission electron microscopy image of the 300°C annealed ordered nanoporous 4wt% Pd-SnO_2 film and b) Enlarged STEM image from one part of a). Energy dispersive X-ray scattering (EDX) line measurement taken through two palladium clusters A and B from the above image shows the presence of Pd, Sn.

Fig. 5A gives more details about the dispersion of palladium inside the nanoporous tin dioxide thin films. It shows that there are few different bright spots with diameter size at less than 2nm on thin film, which are detected as palladium clusters as shown on Fig. 5B. However, these bright spots with palladium nanoparticles are too few and it is difficult to locate distinct palladium nanoparticles on most areas of the films. An EDX line measurement taken from one area on Fig. 5B reveals the presence of palladium and tin, but it is impossible to distinguish palladium with tin dioxide, indicating the fantastic dispersion of palladium all over the thin film. These results imply that the ordered nanoporous thin films possess nice dispersion of palladium.

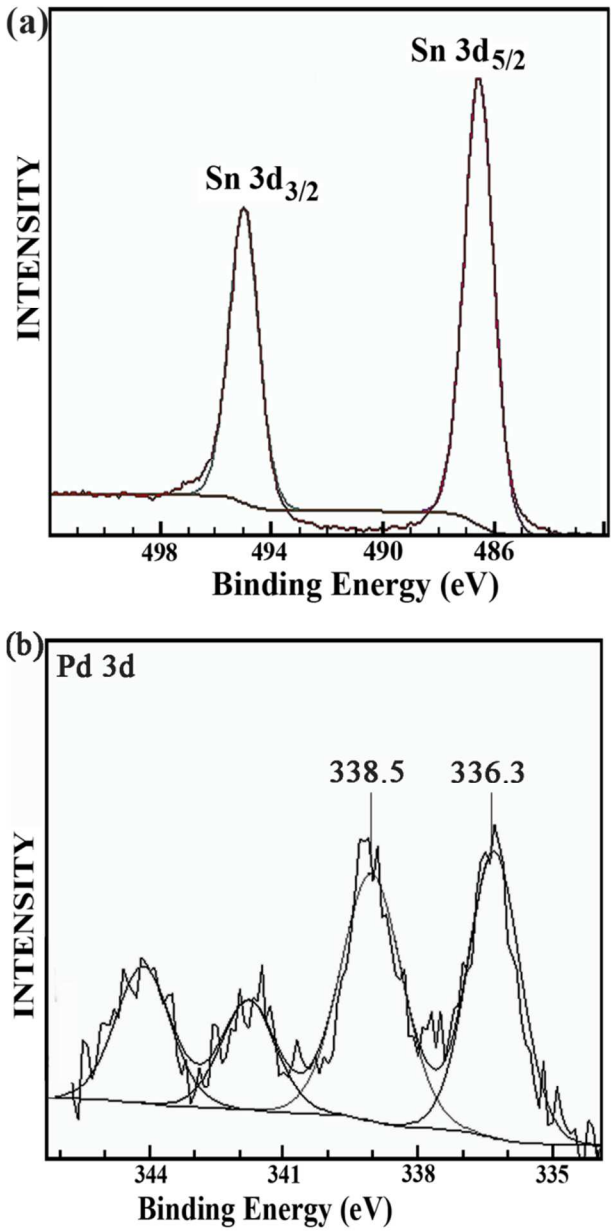

Fig. 6 (a) Sn 3d and (b) Pd 3d spectra of the 300°C annealed ordered nanoporous 4wt% Pd-SnO_2 film.

To get deeper insights in the chemical composition of thin films surface, pure SnO_2 thin films synthesized after 120°C hydrothermal treatment and annealing at 300°C were studied by XPS and the corresponding experimental data are shown in ESI, Fig. S5. In Fig. S5, for hydrothermal treated thin films, all of the features were ascribed to Sn, O, and C elements, and no additional peaks of other atoms were detected. Upon annealing at 300°C, the C 1s peak has dramatically collapsed, and the residual carbon (284.6 eV) peak corresponds to carbon contamination. Furthermore, two symmetric peaks located at 486.5 ± 0.1 and 494.9 ± 0.1 eV were observed for 300°C annealed pure SnO_2 thin films and were assigned to the Sn 3d5/2 and Sn 3d3/2 bands. The Sn 3d5/2 region exhibited a single feature at a binding energy of 486.5 ± 0.1 eV, confirming that the sample was composed of only Sn(IV) states. To further understand the immobilization of Pd on SnO_2 sensing films, the nature of the Pd-SnO_2 interaction was probed by XPS analysis. Chemical compositional analysis of the as-synthesized sensing films was determined by the representative high-resolution XPS spectra comprising Sn 3d, Pd 3d and O 1s core levels of 4wt% Pd-doped SnO_2 sensing film after annealing and sensing test, show in Fig. 6. The Sn 3d core level spectra of Pd-doped thin films shown in Fig. 6a consists of a doublet located a binding energies of 486.5 and 494.9 eV, which can be assigned to the Sn $3d_{5/2}$ and Sn $3d_{3/2}$ of Sn^{4+} in SnO_2, respectively. Analysis of the Sn 3d core level spectrum with Pd dopant displays a binding energy shift of +0.4 eV compared to the E_b of pure SnO_2 particles. This peak shift is attributed to an interaction between Pd and SnO_2, which can give rise to shifts in core level binding energy.[42, 43] XANES that corresponds to an electronic transition from inner electronic levels to outer unoccupied levels gives useful structural information such as oxidation state of chemical species, site symmetry, and covalent bond strength and has widely been used to infer the local structure around the central atom. Sn K-edge normalized XANES of 4wt% Pd doped SnO_2 thin film is shown in ESI, Fig. S6. The position of the edge that is usually taken as the maximum of the first derivative of the XANES spectra can also be used to evaluate the oxidation state of the absorbing atom: a shift toward higher energies is generally attributed to an increased oxidation state of the metal. Compared to the reference sample SnO_2, that have an edge position located at 29 205.3 eV, the 300°C annealed ordered nanoporous 4wt% Pd-SnO_2 film has an identical edge position indicating that tin in this material is likely to be fully oxidized into SnO_2. Moreover this sample features a very similar XANES profile to the bulk cassiterite SnO_2 both in terms of shape and location of the resonance peaks indicating a similar structure.

In Fig. 6b, the Pd 3d core level line could be fitted with two main doublets with the E_b of Pd $3d_{5/2}$ at 336.3 eV and 338.5 eV. The palladium state with the lower E_b can be assigned to Pd^{2+} in palladium oxide (PdO) but with shift to a lower energy by 0.3-0.5 eV in relation to the E_b of bulk PdO, which was expected to smaller oxidized palladium nanoparticles than in case of the bulk oxide. The Pd $3d_{5/2}$ peak with the higher E_b can be assigned to the strongly oxidized palladium (4+) state.[44, 45] PdO_2 is unstable in its anhydrous form but has been shown to be stabilized by the matrix of other oxides, such as SnO_2 and PdO.[46, 47] Therefore, it is reasonable to propose that the Pd^{4+} state in our work is stabilized in its anhydrous form by the SnO_2 oxide. For oxygen element, as shown in Fig. S7 (ESI), the O 1s core level of Pd-doped SnO_2 thin film can be deconvoluted into two contributions centered at 531.9 eV and 530.4 eV, respectively. The main component of O 1s centered at 531.9 may be assigned to the chemisorbed oxygen on SnO_2 surface while the peak located at 530.4eV can be attributed to lattice oxygen (O^{2-}) of Pd-doped SnO_2 lattice on the outermost surface.[48, 49]

3.2 Application to acetone sensing

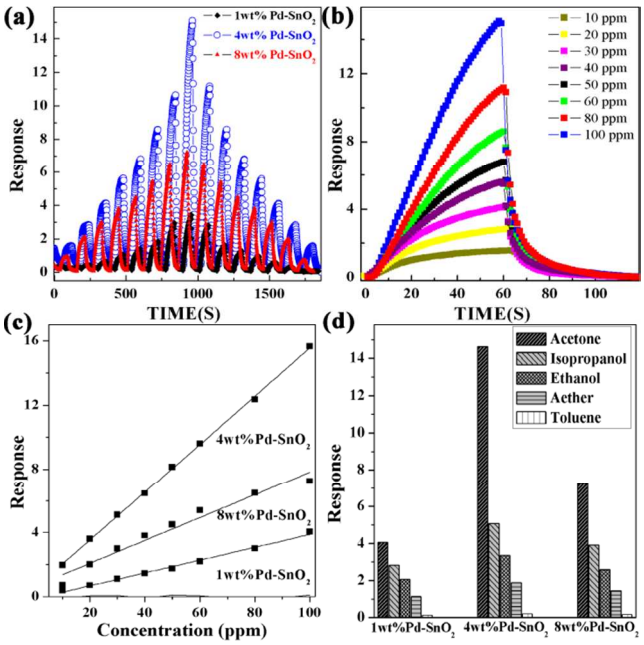

Fig. 7 (a) Response curves of 1wt%, 4wt%, and 8wt% Pd-SnO_2 films sensors measured under various acetone gas concentrations; (b) Typical response and recovery curves of the 4wt% Pd-SnO_2 film sensor to acetone gas at different concentrations; (c) Normalized response of the 1wt%, 4wt%, and 8wt% Pd-SnO_2 films sensors as a function of acetone gas concentrations; (d) Selectivity histograms of sensor responses to 100 ppm of actone, isopropanol, ethanol, aether, andtoluene vapour of 1wt%, 4wt%, and 8wt% Pd-SnO_2 sensors at room temperature.

The structure and morphology of metal oxide materials were reported to have a large effect on their physical, chemical, and application performance. In this work, the ordered nanoporous structure and particle size control of SnO_2 are realized by the improved post hydrothermal treatment, which is expected to bring about more efficient gas sensing performance as compared to conventionally prepared SnO_2 sensing films. On the other hand, metal element doping has also long been proven to be a facile and efficient way to enhance the sensing property of semiconductor metal oxide sensors, because doping can effectively modulate the parameters of the crystal cell and the adsorption of oxygen. In this work, we synthesized the Pd-doped nanoporous SnO_2 with highly ordered nanostructure and researched the metal element doping effect on their gas-sensing properties.

The typical response curves of 1wt% Pd-doped SnO_2, 4wt% Pd-doped SnO_2, and 8wt% Pd-doped SnO_2 based gas sensors measured under various acetone concentrations are shown in Fig. 7a. The response, S, is defined as $(R_{air}-R_{gas})/R_{gas}$ for the reducing gases (acetone) where R_{gas} and R_{air} denote resistance in the presence and the absence of a test gases, respectively. The measurement were performed at room temperature with acetone gas exposure concentration ranging from 10ppm to 100ppm, and the test were switched from low concentration to high concentration, and then conversely from high concentration to low concentration. Upon exposure to acetone, the ordered nanoporous sensing film quickly responds with a decrease in resistance, which reveals the typical n-type semiconducting behaviour of sensing films. Each exposure/recovery cycle were carried out for an exposure interval of 50s followed by a recovery interval of 50s in dry air. A clear increase in the sensor response is observed with the increasing gas concentration, and of all the materials tested, ordered nanoporous 4wt% Pd-SnO_2 sensing film exhibits the best acetone-sensing performance, with high response to acetone concentrations between 10 and 100ppm. The sensor response clearly tracks the change in the acetone concentration, as shown in Fig. 7b. Moreover, the responses are extremely fast, and the sensor can fully recover in very short times after acetone removal. Specifically, the response times, defined as the time necessary to reach 90% of the maximum response, range between 30 and 36 s and decrease as the acetone concentration is increased. The recovery times are in the range of 15-20 s and decreased as the acetone concentration decreased. The repeatability and reproducibility of 4wt% Pd-doped SnO_2 sensor to 20ppm, 40ppm, and 80ppm acetone vapour were evaluated. The sensor responses are stable and reproducible for repeated testing cycles. Each sensor shows good repeatability with less than 5% response variation from four repeated measurements at the same gas concentration, as shown in Fig. S8. The remarkably high response registered in the presence of palladium can be attributed to the catalytic role of the PdO and PdO_2 nanopartilces in promoting the dissociation of molecular acetone at room temperature on the sensing layer. Indeed, the doping of nanoporous thin films with palladium that promote the catalytic decomposition of acetone is a well-known strategy for increasing the sensitivity of the sensing films. [50] The sensor sensitivities of 1wt%, 4wt%, and 8wt% Pd-SnO_2 samples as a function of acetone concentration are provided in Fig. 7c. It can be seen that 4wt% Pd-SnO_2 sample is much more sensitive than the other samples. Taking 100 ppm as an example, 4wt% Pd-SnO_2 sample exhibits a sensitivity of 14.64, which is more than twice higher than that (7.24) of 8wt% Pd-SnO_2 sample. One probable reason is that acetone reacted mainly at the film outer and inner surface due to the strong catalytic activity of PdO and PdO_2. This effect should be more pronounced at higher Pd doping amounts, hindering gas molecules from diffusing deep inside the sensing films. In contrast, at optimal Pd doping amounts at 4wt%, gas molecules can efficiently penetrate within films, generating larger sensor responses by surface reaction, which is catalytically activated by PdO and PdO_2. It should also be pointed out that ordered nanoporous 4wt% Pd-SnO_2 sample also possesses superior performance when compared with other SnO_2-based samples reported in previous works[9, 11, 15], which means that post-synthetic hydrothermal treatment is an effective method to synthesize high sensitivity ordered nanoporous SnO_2 gas sensor. A similar sensitivity could not be observed in the case of a similar nanoporous tin dioxide thin film prepared under similar conditions but without palladium (ESI, Fig.S9)

Selectivity is another very important parameter for the ordered nanoporous SnO_2 gas sensor, because poor selectivity will induce mistaken alarm and limit its extensive utilization. Several vapour organic compounds were tested to explore the potential application of Pd-decorated mesoporous SnO_2 as an excellent sensor in terms of high sensitivity and fast response for chemical vapour detection at room temperature. The responses of the 1wt%,

4wt%, and 8wt% Pd-doped SnO_2 based gas sensors to five target gases with 100ppm concentration at room temperature were further investigated, and the relevant results are shown in Fig. 7d. As the Pd-doping concentration increases from 1 to 4wt%, response to acetone increases rapidly whereas that to isopropanol, ethanol and aether also increases but with a much smaller rate, and those to toluene are not significantly changed, indicating the significant enhancement of the acetone selectivity with increasing palladium doping level. That is to say, the present sensors display quite outstanding selectivity to acetone, especially the Pd-doped SnO_2, of which the responses reach 5.07, 3.36, 1.88, and 0.2 to isopropanol, ethanol, aether, and toluene, respectively. At the optimal palladium doping level of 4 wt %, the acetone response becomes about 3 times as high as that to ethanol. Thus, 4 wt % Pd-doped SnO_2 thin film exhibits not only high response but also high acetone selectivity against ethanol and other gases at a low gas concentration of 100 ppm. It is important to note that the highest response to acetone of 4wt% Pd-doped SnO_2 based sensors is possibly due to the difference in the interaction between target gas molecules and the surface of sensor materials. At the measured temperature, the pre-adsorbed oxygen on the surface of sensing material is favoured for the interaction with acetone.[51] Therefore, when exposure to acetone, the number of free electrons released back to the sensing layer was high, leading to a large resistance change. As a result, the 4wt% Pd-doped SnO_2 based sensors show the highest sensitivity to acetone. At higher Pd doping levels (8wt%), the acetone response reduces substantially compared with the optimally doped one. The unfavourable characteristic may be caused by the high-level surface disorder on sensing films surfaces induced by the heavy Pd doping. The surface disorder can be represented as defective surface states that trap charge carries, causing pinning of Fermi-level, less change of surface conductivity due to charge transfer from reducing reaction and deteriorated gas response.[52] However, more in-depth studies are necessary to understand the selective behaviour of such ordered nanoporous sensing films to acetone among many VOCs.

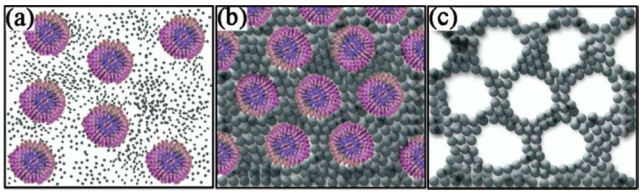

Scheme 1 Directly after spin coating and drying at 60 °C (a) micelles are irregularly arranged and in between single precursor units are dispersed. (b) Upon the post-synthetic water vapour treatment at 120 °C, the inorganic precursor condenses between the micelles arranging in a more ordered fashion. Uniformly sized crystalline nanoparticles are formed between the micelles stabilizing for the structure that upon template removal the crystalline particles slightly grow but only a small shrinkage of the pores normal to the surface can be observed(c).

In cases where a nanoporous structure can be obtained the structure is not necessarily stable for the transformation into a nanoporous thin film. Most metal oxides crystallize during the thermal removal of the template or degrade upon extraction procedures. The reason is the lacking support of the structure director after its removal. The strong forces that occur during the nucleation and crystal growth in the pore walls are not compensated and lead to a complete loss of structure. Two possible direct solutions for this problem were introduced in the past: (i) the application of structure directors that are thermally more stable and are removed after the crystallization of the inorganic framework is completed[41] and (ii) special post-synthetic treatments like the delayed humidity treatment (DHT)[53, 54] which are applied on thin films that do not exhibit a mesostructure directly after the spin or dip coating. The first approach only works for metal oxides that crystallize below the templates thermal decomposition temperature and has the disadvantage of very expensive and commercially not available templates. In contrast, the second approach utilizes commercially available templates but usually results in thermally less stable thin films. We show a new synthetic approach that overcomes the problems for the so far established methods in Scheme 1. To attain better control over the post-synthetic hydrothermal procedure, we used a climate controlled chamber that gave precise control over hydrothermal conditions (e.g., temperature, humidity, and evaporation times). It allows the synthesis of Pd-SnO_2 thin films with ordered nanopores at low temperature. Furthermore, tin dioxide crystalline pore walls can be achieved at low temperatures of 120 °C allowing an easy thermal removal of the template by calcination without loss of nanoporous structure or significant shrinkage of the thin film normal to the substrate. In addition, the crystalline pore walls are thin (about 9-12nm) and the size of 4wt% Pd doped SnO_2 grains mainly range from 3 to 4 nm. It indicates that the thickness of the pore wall is approximately equal to the size of 3-4 SnO_2 grains. K. K. Khun *et al.* have reported that SnO_2 alone exhibited conductivity that was too low and did not display a detectable response to acetone vapour at room temperature[14], while our work suggests that the highly ordered Pd doped SnO_2 sensing films can be a potential pathway to achieve room temperature gas sensing with better sensing performance than their constituents alone. The gas sensing mechanism of ordered nanoprous sensing films can be explained by the surface-depletion model. When the ordered nanoporous sensing film is exposed to dry air, oxygen ions are adsorbed onto the sensing film surface. Therefore, the depletion layer may extend throughout the whole area of the sensing films nanostructure, which leads to high resistance. On the other hands, upon exposure to reducing gas such as acetone, gas molecules will react with the chemisorbed oxygen ions at the sensing film surface to form CO_2 and H_2O. This increases the charge carrier concentration in the sensing film pore walls and narrows the surface depletion layer width, which leads to decrease in the resistance of the ordered nanoporous sensing films.

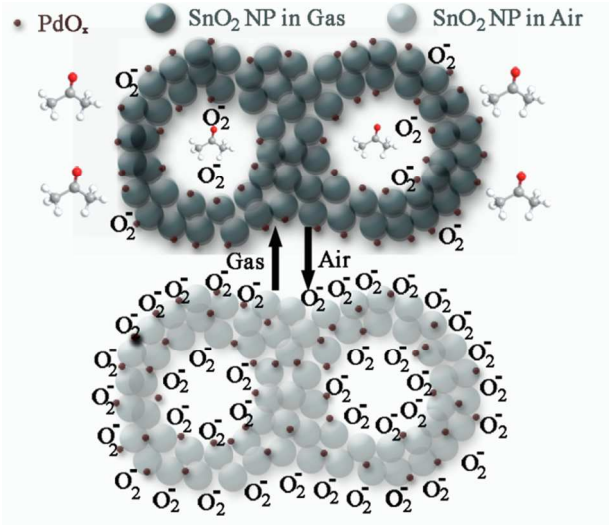

Scheme 2 Response mechanism of ordered nanopore and pore wall exposed to reducing gases or air.

Scheme 2 shows the adsorption illustration of acetone gas molecules adsorbed onto the sensing films. Chemisorbed oxygen molecules in the atmosphere are ionized to oxygen ions through the capture of free electrons from the surface of SnO_2 pore walls (eqn (1) and (2)). Lai and Wang et al. separately reported that particle size and morphology of metal oxide materials had great influence on their thickness of electron depletion layer and diffusion of gas molecules during the gas sensing.[35, 55] In our Pd doped SnO_2 based sensors, since the grain size (D~3.2nm) is much close to L, where L is the width of the space charge region (that is Debye length, ~3nm for SnO_2) due to the chemisorption-induced oxygen surface states,[56] the depletion layer has extended to cover the whole region of the grains and enables a strong grain size effect, which means the whole SnO_2 sensing films is completely depleted. When the sensor is exposed to a reducing gas such as acetone gas, the gas molecules react with the oxygen ions on the surface of sensing films, as shown in eqn (3)-(5).[15] Such reactions result in the retrieval of the trapped electrons back to the conduction band of the sensing film and lead to a decrease in resistance for the gas sensor.[57, 58] As a result, the ordered nanoporous 4wt% Pd-SnO_2 sensing films with 3.2 nm particle size showed the highest sensitivity and excellent selectivity, compared with the other samples.

$$O_{2(gas)} \rightarrow O_{2(adsorbed)} \quad (1)$$

$$O_{2(adsorbed)} + e^- \rightarrow O_2^- \quad (2)$$

$$CH_3COCH_3 + O_2^- \rightarrow CH_3C^+O + CH_3O^- + e^- \quad (3)$$

$$CH_3C^+O \rightarrow CH_3^+ + CO \quad (4)$$

$$CO + O_2^- \rightarrow CO_2 + e^- \quad (5)$$

4. Conclusions

Highly organized, transparent, crystalline nanoporous Pd-doped SnO_2 thin films are obtained through a 120 °C post-synthetic hydrothermal treatment of the as-deposited film. Characterizations by XRD, SEM, TEM, HRTEM, Raman spectroscopy and XPS reveal that Pd-doped SnO_2 thin film obtained highly ordered nanostructure, highly crystalline tin oxide of cassiterite structure, small particle size, and outstanding particle interconnectivity. The ordered nanoporous structure allows for rapid gas diffusion throughout the thin film. The small grain size of the nanocrystal subunits and the three-dimensional interconnected nanoporous structure are responsible for the dramatically improved electrochemical properties of SnO_2 thin films. Pd doping further increases the sensor response due to the catalytic and electrical sensitization effects of PdO and PdO_2. The optimization of the synthesis parameters and the conditions of post-synthetic hydrothermal treatments lead to materials differing significantly in the physicochemical properties and their sensing behaviour. The best results with respect to porosity, nanostructural ordering, as well as the sensing behaviour are obtained by the tin dioxide thin films doped with 4 wt% palladium prepared with spin-coating at 30% relative humidity, aging for 2 h at 60°C, for 12 h at 120°C and 95% relative humidity and gradual calcination at 300°C. The acetone response of the SnO_2 sensing film with 4 wt% Pd-doping level is found to be substantially improved up to 14.64 at 100 ppm with a short response time of ~30 s at room temperature. The enhanced acetone-sensing performances of Pd-doped SnO_2 thin films may be attributed to large specific surface area of the nanostructure, specifically high interaction between acetone vapour and sensing film surface, and small grain size. In general the synthesis procedure described in this report has the advantage of being easy, cost efficient, highly reproducible and therefore highly suitable for the fabrication of high performance ordered nanoporous crystalline materials for applications including gas sensing, photocatalysis, and 3rd generation photovoltaics.

5. Acknowledgments

This work was supported by the Startup Foundation for Introducing Talent of NUIST and the grant of Specially-Appointed Professor of Jiangsu. We thank the Siemens AG for the helping in the design, preparation and donation of the sensor devices. We thank the University of Munich and especially Prof. Dr. T. Bein for his constant support.

Notes

[a] *Department of Materials Physics, School of Physics and Optoelectronic Engineering, Nanjing University of Information Science &Technology, Nanjing, China. Fax: +86-025-58731031; Tel: +86-025-58731031; E-mail: ssfshao@nuist.edu.cn*
[b] *Department of Chemistry & Biochemistry, University of Munich, Munich, Germany.*
† Electronic Supplementary Information (ESI) available: See DOI: 10.1039/b000000x/

References

1. H. Nguyen and S. A. El-Safty, *J. Phys. Chem. C* 2011, **115**, 8466.
2. S. Li, T. Liu, Y. Zhang, W. Zeng, F. Pan and X. Peng, *Mater. Lett.* , 2015, **143**, 12.
3. W. Q. Li, S. Y. Ma, J. Luo, Y. Z. Mao, L. Cheng, D. J. Gengzang, X. L. Xu and S. H. Yan, *Mater. Lett.* , 2014, **132**, 338.
4. I. Lee, S.-J. Choi, K.-M. Park, S. S. Lee, S. Choi, I.-D. Kim and C. O. Park, *Sens. Actuators, B* 2014, **197**, 300.
5. S. J. Choi, I. Lee, B. H. Jang, D. Y. Youn, W. H. Ryu, C. O. Park and I. D. Kim, *Anal. Chem.*, 2013, **85**, 1792.
6. Z. Guo, J. Liu, Y. Jia, X. Chen, F. Meng, M. Li and J. Liu, *Nanotechnology*, 2008, **19**, 345704.
7. X. Sun, H. Hao, H. Ji, X. Li, S. Cai and C. Zheng, *ACS Appl. Mater. Interfaces*, 2014, **6**, 401.
8. T. Kida, T. Doi and K. Shimanoe, *Chem. Mater.*, 2010, **22**, 2662.
9. S. Singkammo, A. Wisitsoraat, C. Sriprachuabwong, A. Tuantranont, S. Phanichphant and C. Liewhiran, *ACS Appl. Mater. Interfaces*, 2015, **7**, 3077.
10. C. Shao, Y. Chang and Y. Long, *Sens. Actuators, B* 2014, **204**, 666.
11. J. K. Srivastava, P. Pandey, V. N. Mishra and R. Dwivedi, *J. Nat. Gas Chem.*, 2011, **20**, 179.
12. L. K. Bagal, J. Y. Patil, K. N. Bagal, I. S. Mulla and S. S. Suryavanshi, *Mater. Res. Innovations* 2013, **17**, 98.
13. L. Cheng, S. Y. Ma, X. B. Li, J. Luo, W. Q. Li, F. M. Li, Y. Z. Mao, T. T. Wang and Y. F. Li, *Sens. Actuators, B* 2014, **200**, 181.
14. K. K. Khun, A. Mahajan and R. K. Bedi, *J. Appl. Phys.*, 2009, **106**, 124509.
15. D. Zhang, A. Liu, H. Chang and B. Xia, *RSC Advances*, 2015, **5**, 3016.
16. P. D. Yang, D. Y. Zhao, D. I. Margolese, B. F. Chmelka and G. D. Stucky, *Nature*, 1998, **396**, 152.
17. B. Z. Tian, X. Y. Liu, B. Tu, C. Z. Yu, J. Fan, L. M. Wang, S. H. Xie, G. D. Stucky and D. Y. Zhao, *Nat. Mater.*, 2003, **2**, 159.
18. J. Fan, S. W. Boettcher and G. D. Stucky, *Chem. Mater.*, 2006, **18**, 6391.
19. H.-P. Cong and S.-H. Yu, *Cryst. Growth Des.*, 2009, **9**.
20. J. Zhang, S. Wang, M. Xu, Y. Wang, B. Zhu, S. Zhang, W. Huang and S. Wu, *Cryst. Growth Des.*, 2009, **9**, 3532.
21. X. H. Liu, J. Zhang, X. Z. Guo, S. H. Wu and S. R. Wang, *Nanotechnology*, 2010, **21**, 095501.
22. S. Ahmad, B. Jousseaume, L. Servant, T. Toupance and C. Zakri, *Chemical communications*, 2011, **47**, 5001.
23. L. Renard, H. Elhamzaoui, B. Jousseaume, T. Toupance, G. Laurent, F. Ribot, H. Saadaoui, J. Brötz, H. Fuess, R. Riedel and A. Gurlo, *Chem. Commun.*, 2011, **47**, 1464.
24. L. Renard, O. Babot, H. Saadaoui, H. Fuess, J. Brötz, A. Gurlo, E. Arveux, A. Klein and T. Toupance, *Nanoscale*, 2012, **4**, 6806.
25. L. Renard, J. Brotz, H. Fuess, A. Gurlo, R. Riedel and T. Toupance, *ACS applied materials & interfaces*, 2014, **6**, 17093.
26. C. Xu, J. Tamaki, N. Miura and N. Yamazoe, *Sens. Actuators B*, 1991, **3**, 147.
27. N. Yamazoe and K. Shimanoe, *J. Electrochem. Soc.*, 2008, **155**, J85.
28. N. Yamazoe and K. Shimanoe, *J. Electrochem. Soc.*, 2008, **155**.
29. M. Yuasa, T. Kida and S. Kengo, *ACS Appl. Mater. Interfaces*, 2012, **4**, 4231.
30. V. Krivetskiy, A. Ponzoni, E. Comini, S. Badalyan, M. Rumyantseva and A. Gaskov, *Electroanalysis*, 2010, **22**, 2809.
31. D. Koziej, M. Hübner, N. Barsan, U. Weimar, M. Sikora and J. D. Grunwaldt, *Phys. Chem. Chem. Phys.*, 2009, **11**, 8620.
32. K. Suematsu, Y. Shin, Z. Hua, K. Yoshida, M. Yuasa, T. Kida and K. Shimanoe, *ACS Appl. Mater. Interfaces*, 2014, **6**, 5319.
33. N.-L. Wu, S.-Y. Wang and I. A. Rusakova, *Science*, 1999, **285**, 1375.
34. L. Jia, W. Cai and H. Wang, *Appl. Phys. Lett.* , 2010, **96**, 103115.
35. X. Y. Lai, D. Wang, N. Han, J. Du, J. Li, C. J. Xing, Y. F. Chen and X. T. Li, *Chem. Mater.*, 2010, **22**, 3033.
36. M. N. Rumyantseva, A. M. Gaskov, N. Rosman, T. Pagnier and J. R. Morante, *Chem. Mater.*, 2005, **17**, 893.
37. Y. Liu, C. Zheng, W. Wang, C. Yin and G. Wang, *Adv. Mater.*, 2001, **13**, 1883.
38. J. X. Zhou, M. S. Zhang, J. M. Hong and Z. Yin, *Solid State Commun.* , 2006, **138**, 242.
39. A. Sonnauer, F. Hoffmann, M. Fr€oba, L. Kienle, V. Duppel, M. Thommes, C. Serre, G. Ferey and N. Stock, *Angew. Chem., Int. Ed.*, 2009, **48**, 3791.
40. T. Takeguchi, O. Takeoh, S. Aoyama, J. Ueda, R. Kikuchi and K. Eguchi, *Appl. Catal., A*, 2003, **252**, 205.
41. T. Brezesinski, A. Fischer, K.-i. Iimura, C. Sanchez, D. Grosso, M. Antonietti and B. M. Smarsly, *Adv. Funct. Mater.*, 2006, **16**, 1433.
42. D. D. Frolov, Y. N. Kotovshchikov, I. V. Morozov, A. I. Boltalin, A. A. Fedorova, A. V. Marikutsa, M. N. Rumyantseva, A. M. Gaskov, E. M. Sadovskaya and A. M. Abakumov, *J. Solid State Chem.*, 2012, **186**, 1.
43. W. R. Schwartz and L. D. Pfefferle, *J. Phys. Chem. C*, 2012, **116**, 8571.
44. E. P. Domashevskaya, S. V. Ryabtsev, S. Y. Turishchev, V. M. Kashkarov, Y. A. Yurakov, O. A. Chuvenkova and A. V. Shchukarev, *J. Struct. Chem.*, 2008, **49**, 80.
45. Y. Sohn, D. Pradhan and K. T. Leung, *ACS Nano*, 2010, **4**, 5111.
46. L. S. Kibis, A. I. Titkov, A. I. Stadnichenko, S. V. Koscheev and A. I. Boronin, *Appl. Surf. Sci.*, 2009, **255**, 9248.
47. J. Kappler, N. Bârsan, U. Weimar, A. Dièguez, J. L. Alay, A. Romano-Rodriguez, J. R. Morante and W. F. Göpel, *J. Anal. Chem.* , 1998, **361**, 110.
48. J. C. Dupin, D. Gonbeau, P. Vinatier and A. Levasseur, *Phys. Chem. Chem. Phys.*, 2000, **2**, 1319.
49. W. Azelee, W. A. Bakar, M. Y. Othman, R. A. C. K. Yong and S. Toemen, *Mod. Appl. Sci.*, 2009, **3**, 35.
50. P. A. Russo, N. Donato, S. G. Leonardi, S. Baek, D. E. Conte, G. Neri and N. Pinna, *Angew. Chem. Int. Ed.* , 2012, **51**, 11053.
51. Y. Zeng, T. Zhang, M. Yuan, M. Kang, G. Lu, R. Wang, H. Fan, Y. He and H. Yang, *Sens. Actuators, B*, 2009, **143**, 93.
52. G. Korotcenkov, I. Boris, V. Brinzari, S. H. Han and B. K. Cho, *Sens. Actuators, B*, 2013, **182**, 112.
53. J. H. Pan, S. Y. Chai, C. Lee, S. E. Park and W. I. Lee, *J. Phys. Chem. C*, 2007, **111**, 5582.
54. C. Sinturel, M. Vayer, M. Morris and M. A. Hillmyer, *Macromolecules*, 2013, **46**, 5399.
55. L. L. Wang, T. Fei, Z. Lou and T. Zhang, *ACS Appl. Mater. Interfaces*, 2011, **3**, 4689.
56. H. Ogawa, M. Nishikawa and A. Abe, *J. Appl. Phys.*, 1982, **53**, 4448.
57. X. J. Luo, Z. Lou, L. L. Wang, X. J. Zheng and T. Zhang, *New J. Chem.*, 2014, **38**, 84.
58. W. Tang, J. Wang, Z. Liu, Q. Qiao and X. Li, *J Mater Sci*, 2015, **50**, 2605.

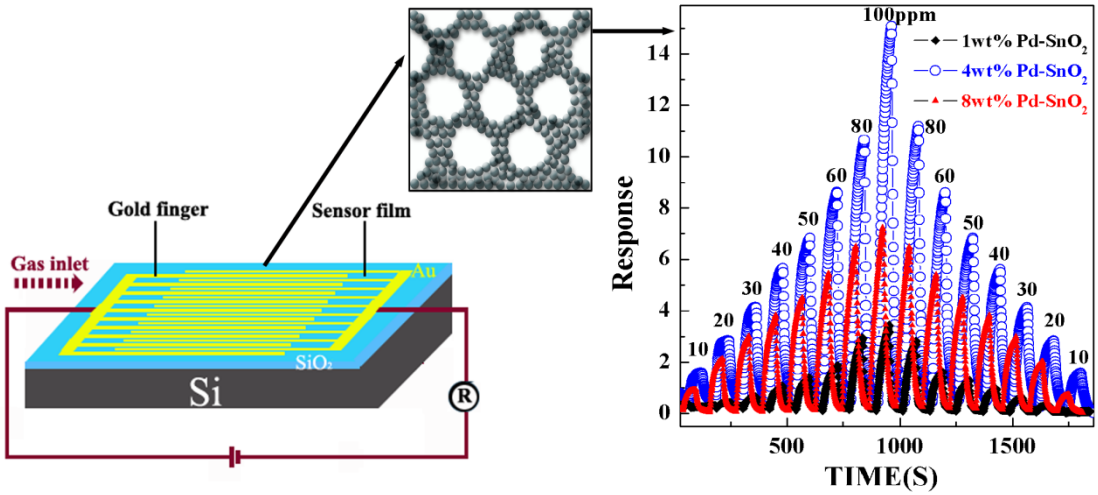

Gas sensing with highly ordered nanoporous materials is attracting much attention because of its promising capability of detecting toxic gases at room temperature. In this study, highly organized, transparent, crystalline nanoporous Pd-doped SnO_2 thin films are obtained through a 120 ℃ post-synthetic water vapour hydrothermal treatment of the as-deposited film. Characterizations by XRD, SEM, TEM, HRTEM, Raman spectroscopy and XPS reveal that Pd-doped SnO_2 thin film obtained highly ordered nanostructure, highly crystalline tin oxide of cassiterite structure, small particle size, and outstanding particle interconnectivity. The best results with respect to porosity, nanostructured ordering, as well as the sensing behaviour are obtained by the tin dioxide thin films doped with 4 wt% palladium prepared with spin-coating at 30% relative humidity, aging for 2 h at 60 ℃, for 12 h at 120 ℃ and 95% relative humidity and gradual calcination at 300 ℃. The acetone response of the SnO_2 sensing film with 4 wt% Pd-doping level is found to be substantially improved up to 14.64 at 100 ppm with a short response time of ~30 s at room temperature. In general the synthesis procedure described in this report has the advantage of being easy, cost efficient, highly reproducible and therefore highly suitable for the fabrication of high performance ordered nanoporous crystalline materials for applications including gas sensing, photocatalysis, and 3rd generation photovoltaics.